

# Volumetric integration model of the Stiles-Crawford effect of the first kind and its experimental verification

**Brian Vohnsen**

Advanced Optical Imaging Group, School of Physics,  
University College Dublin, Dublin, Ireland



**Alessandra Carmichael**

Advanced Optical Imaging Group, School of Physics,  
University College Dublin, Dublin, Ireland



**Najnin Sharmin**

Advanced Optical Imaging Group, School of Physics,  
University College Dublin, Dublin, Ireland



**Salihah Qaysi**

Advanced Optical Imaging Group, School of Physics,  
University College Dublin, Dublin, Ireland



**Denise Valente**

Advanced Optical Imaging Group, School of Physics,  
University College Dublin, Dublin, Ireland



The integrated Stiles-Crawford function is commonly used as apodization model for vision through the natural eye pupil. However, this method does not account for possible effects related to the retinal thickness, the large length-to-diameter aspect ratio of the photoreceptors, or the use of nonMaxwellian illumination. Here, we introduce a geometrical optics model to calculate the fraction of overlap between light at the retina and the photoreceptor outer segments where absorption triggers vision. The model, which does not account for photoreceptor waveguiding, is discussed for both Maxwellian and nonMaxwellian illumination. The integrated Stiles-Crawford effect is analyzed experimentally with a uniaxial pupil-size flicker methodology and we find that the psychophysical measurements match better to the geometrical optics predictions than direct integration of a Stiles-Crawford function.

subjective visibility is determined, using either a bipartite or flickering configuration, with respect to a reference light that enters near the pupil center. The resulting distribution is typically fitted to a rotationally-symmetric Gaussian function  $\eta_{SCE}(r) = 10^{-\rho r^2}$  where  $r$  is the distance in the pupil plane from the point of highest visibility and  $\rho$  is a wavelength-dependent directionality parameter (Stiles, 1937).

Analysis of the SCE with Maxwellian view has overshadowed experimental approaches to SCE integration although only the latter corresponds to normal vision. It is commonly assumed that the SCE function,  $\eta_{SCE}$ , can be integrated for the full pupil despite of the fact that retinal illumination conditions differ significantly in the two cases (Enoch & Lakshminarayanan, 2009) and that aberrations play a role (Vohnsen, 2007). The effective obliqueness of light at the retina is determined by the direction of the Poynting vector at any point (Vohnsen & Rativa, 2011; Westheimer, 2013) but it remains a challenge to infer the actual visual impact of the SCE. Stiles and Crawford stated that “a more detailed study of this point would, however, be useful” (Stiles & Crawford, 1933); but only few have dealt with it rigorously such as, for example, the use of multiple Maxwellian pupil entrance points and annular rings (Drum, 1975; Ercoles, Ronchi, & Toraldo di Francia, 1956), coherent light integration (Castillo & Vohnsen, 2013; Vohnsen & Rativa, 2011), and blur and integration (Enoch, 1958). Previous studies have been somewhat inconclusive reporting both over- and

## Introduction

The Stiles-Crawford effect of the first kind (SCE) describes a psychophysically-determined reduction in light-capture efficiency of visual pigments to obliquely incident light on the retina (Stiles & Crawford, 1933). It is normally analyzed using Maxwellian view where light enters the eye through a point that is scanned sequentially across the pupil (Applegate & Lakshminarayanan, 1993; Lochocki & Vohnsen, 2013). The

Citation: Vohnsen, B., Carmichael, A., Sharmin, N., Qaysi, S., & Valente, D. (2017). Volumetric integration model of the Stiles-Crawford effect of the first kind and its experimental verification. *Journal of Vision*, 17(12):18, 1–11, doi:10.1167/17.12.18.

doi: 10.1167/17.12.18

Received July 4, 2017; published October 31, 2017

ISSN 1534-7362 Copyright 2017 The Authors



This work is licensed under a Creative Commons Attribution-NonCommercial-NoDerivatives 4.0 International License.

Downloaded From: <http://jov.arvojournals.org/> on 04/19/2018

underadditivity with the test appearing dimmer (Stiles & Crawford, 1933) or brighter (Enoch, 1958) than predicted by an integrated SCE.

It is well known that photoreceptors have directional properties evidenced by microscopy studies of light transmission by cones and rods (Enoch, 1963; Packer, Williams, & Bensinger, 1996). This has led to a number of waveguide-based models using analogies with optical fibers (Snyder & Pask, 1973; Vohnsen, Iglesias, & Artal, 2005). Nonetheless, it must be stressed that the transmitted light has not been absorbed by visual pigments and thus it would not contribute to vision in the eye. The small fraction of backscattered light used for high-resolution fundus imaging is caused by refractive index inhomogeneities and, although directional, does not contribute to vision either (Rativa & Vohnsen, 2011; Roorda & Williams, 2002). The occurrence of internal outer-segment reflections in optical coherence tomography is indicative of axial refractive index alterations that perturb light guiding (Pircher, Götzinger, Sattmann, Leitgeb, & Hitzenberger, 2010). Also, the dense stacking of membrane invaginations and visual pigments modulate the outer segment refractive index axially to increase its effective value. As a result, one of the authors recently suggested that waveguiding may not be as fundamental for vision as commonly assumed (Vohnsen, 2014, 2017). The short length of photoreceptors, their packing and structural variations, will inevitably degrade their guiding capabilities, and the lack of effective absorption between outer segments makes it questionable whether nonguided light components can be effectively dampened without contributing to vision. This is exemplified by the self-screening explanation of the hue shift identified as the Stiles-Crawford effect of the 2nd kind (Stiles, 1937; Vohnsen, 2017), the spectral dependence of the directionality (Walraven & Bouman, 1960) and possible leakage of light between photoreceptors in the transient Stiles-Crawford effect (Chen & Makous, 1989; Lochocki & Vohnsen, 2017). Moreover, waveguide models fall short of explaining why only cones show a marked SCE directionality whereas rods do not (Van Loo & Enoch, 1975).

Complementary to psychophysical measurements, objective methods can determine a related optical SCE that has been examined via pupil imaging (Burns, Wu, Delori, & Elsner, 1995; Gorrand & Delori, 1995; van Blokland, 1986), fundus photography (Morris et al., 2015; Roorda & Williams, 2002), scanning laser ophthalmoscopy (Delint, Berendschot, & van Norren, 1997; Rativa & Vohnsen, 2011) and optical coherence tomography (Gao, Cense, Zhang, Jonnal, & Miller, 2008). Scattering and waveguiding (Marcos & Burns, 1999; Marcos, Burns, & He, 1998) or waveguide diffraction has been used to model this case (Vohnsen, Iglesias, & Artal, 2005). The major reflective element within the photore-

ceptors is the high-index mitochondria packed densely in the ellipsoid. This scattered light does not contribute significantly to vision triggered by absorption in the outer segments although a characteristic optical SCE directionality parameter can still be determined (Marcos, Burns, & He, 1998; Morris et al., 2015).

In this study, we propose a new geometrical optics model for vision that is based on the volumetric overlap between the illumination and outer segment visual pigments without including waveguiding. Electromagnetic light propagation and absorption in the visual pigments will ultimately give a more accurate description (Vohnsen, 2014), but a geometrical optics model is intuitively more appealing. We discuss the geometrical overlap predictions both for the integrated SCE and for conventional Maxwellian illumination. Finally, an experimental verification of the integrated SCE is described. The system is uniaxial and makes use of alternating pupil sizes for subjective determination of effective visibility. Experimental results obtained with five subjects (the authors) are compared with the geometrical predictions and with analytical integration of a Gaussian SCE.

The paper is organized as follows: In the following section, the optical models are described. The next section contains the experimental method for direct determination of the integrated SCE. Then these experimental results are discussed and compared to the model predictions in the subsequent section, and finally, in the last section, we present our conclusions.

## Geometrical optics model

It is important to estimate the fraction of energy that falls within the outer segments since this determines the visibility. In the retina the density of visual pigments is not high. Typical foveal values from the literature are 0.3 for M and L cones (Bowmaker & Dartnall, 1980; Elsner, Burns, & Webb, 1993; Kilbride, Read, Fishman, & Fishman, 1983) and only about 0.1 for the S cones (Wysecki & Stiles, 1980) that are entirely absent or rare in the central 25' fovea (Williams, MacLeod, & Hayhoe, 1981). Pigment densities reduce with eccentricity (Kilbride, Read, Fishman, & Fishman, 1983) and show also some age dependence (Elsner, Berk, Burns, & Rosenberg, 1988). Accordingly, only a small fraction (< 30%) of the incident light will be absorbed by visual pigments. The fraction of absorbed light is proportional to the effective visibility,  $\eta_{eff}$ , and for a single ray it can be expressed via Beer-Lambert's law

$$\eta_{eff} \propto 1 - \exp(-\alpha L) \approx \alpha L - (\alpha L)^2/2 + (\alpha L)^3/6 - \dots \quad (1)$$

where  $L$  is the total propagation length across

(uniform) material with absorption coefficient  $\alpha = N\sigma_{abs}$ ,  $N$  is the molecular density and  $\sigma_{abs}$  is the molecular absorption cross section. When the absorption by visual pigments is low, only a fraction of the light will trigger vision and, to a first approximation, it scales with the intersection volume. In this limit  $\alpha L \ll 1$ , and Equation 1 is linear.

The geometrical optics model is divided into three parts: First, the overlap between light at the retina and the foveal cones is modeled by the intersection volume of focused light spreading across the outer segments for vision through the normal pupil. The second part discusses Maxwellian illumination. The third summarizes integration of the standard Gaussian SCE. The effective visibility is estimated as the ratio of the intersection volume of the conical illumination and cylindrical outer segments,  $V_{intersect}$ , with respect to the volume of the illumination itself,  $V_{light}$ , i.e.,

$$\eta_{eff} = V_{intersect}/V_{light}. \quad (2)$$

This ensures normalization had visual pigments been present everywhere across the illuminated retina.

For a schematic eye with  $f_{eye} = 22.2$  mm the angle of incidence at the retina,  $\theta$ , is related to a pupil point,  $r$ , via  $\theta \approx r/f_{eye}$ . The dimensions and spacing of foveal cone outer segments varies. The L and M foveal cones have an outer segment length  $L_{outer}$  in the range of 50–60  $\mu\text{m}$  whereas S cone outer segments are slightly shorter. The foveal outer segment diameter  $d_{outer}$  is in the range 1.5–2.0  $\mu\text{m}$ . The density of foveal cones is approximately 160,000–200,000/mm<sup>2</sup> (Curcio, Sloan, Kalina, & Hendrickson, 1990) which for a hexagonal packing corresponds to a center-to-center spacing  $d_{spacing}$  in the range 2.4–2.7  $\mu\text{m}$ .

### Volumetric overlap model in normal vision (nonMaxwellian)

For a conical beam focused onto a single, cylindrical outer segment, the intersection volume can be calculated analytically. The model is shown schematically in Figure 1 for a single illuminated point on the retina with straight rays across the outer segments and a slight leakage to neighboring outer segments. This model is plausible if waveguiding is ineffective. Reported refractive indices from literature (Sidman, 1957; Snyder & Pask, 1973) suggests critical angles of  $\sim 82^\circ$  and  $\sim 70^\circ$  within the inner and outer segments corresponding to oblique incidence angles of  $8^\circ$  and  $20^\circ$ , respectively. Irregular cellular surfaces and internal refractive variations will degrade the effectiveness of light guiding. In photoreceptor cells light may be focused near the inner segment entrance (not shown in Figure 1), but the elevated refractive index of mitochondria in the ellipsoid will partially redirect this light onto the

outer segment and has been proposed to provide impedance matching between inner and outer segments (Toraldo di Francia, 1948). Moreover, light incident between the photoreceptors (or through photoreceptors without being absorbed) will potentially traverse adjacent cells. The slight elevation of the refractive index across the photoreceptors will still make transmitted light directional but at the short distances across the retina will not effectively diminish nonguided light (dos Santos & Vohnsen, in press).

Rays are confined within individual outer segments if entering the eye through a small pupil  $d_{pupil} = f_{eye}d_{outer}/L_{outer}$  which for foveal cones equals 0.6–0.9 mm. For the shorter parafoveal cones ( $L_{outer} \sim 20\text{--}30 \mu\text{m}$ ), the angular spread of rays confined within the outer segments is approximately matched to the natural pupil size. Consequently, only a tiny fraction of the light can enter adjacent photoreceptors unless the pupil is large. These neighboring cells will be less likely to absorb the light both due to the smaller intersection volume and the possibility that they belong to a different cone class. Light may strike the outer segment at any point on or off axis or between the cells. Thus, the overlap is that between a single or multiple outer segments and a beam of light represented by a truncated cone with apex size equal to the circle enclosing the outer segments and apex angle set by the angular limit of the contributing rays. The intersection volume equals the total volume of illuminated outer segments and the effective visibility is the ratio with respect to the volume of the light beam. To ease visualization we have implemented the volumetric overlap integral numerically in COMSOL<sup>TM</sup>. Figure 2 shows the overlap between a cone of light with respectively one and seven adjacent identical outer segments.

Figure 3 shows the resulting effective visibility calculated from Equation 2 and normalized to a 1.4 mm pupil (as used in the experiments discussed in Sec. 3) for outer segments of slightly different length and diameter with outer segments acting individually or in groups of seven, 19, or 37 identical adjacent outer segments containing the same type of visual pigment. The effective visibility drops off slightly faster with increasing pupil size for smaller outer segment diameter and/or increasing outer segment length.

### Volumetric overlap model for standard SCE characterization (Maxwellian)

The same geometrical model can be applied to Maxwellian illumination analysis of the SCE with COMSOL<sup>TM</sup> as illustrated in Figure 4. An elongated hexagonal prism has been implemented as illumination model representative of a collimated plane-wave illumination (a cylindrical beam gives almost identical results), and its intersection volume with one or



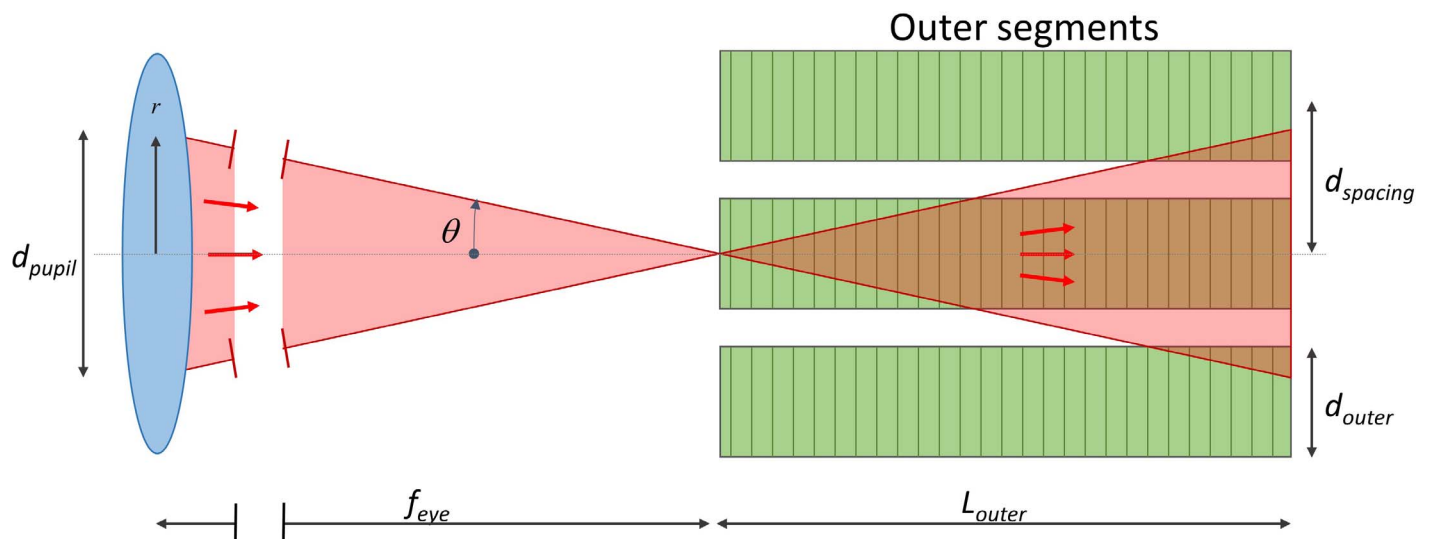


Figure 1. Volumetric overlap model for absorption in outer segments. Light reaches the outer segment as a conical beam that diverges again across the outer segments. The schematic representation of the focused light represents the angular spread of wavevectors that contribute to the point-spread-function at the retina.

multiple cylindrical outer segments has been determined at different angles of incidence. The end face of the illumination prism has been chosen to match the filling area of the outer segments including the intracellular space. The beam has been rotated about the midpoint of the outer segment, or group of outer segments. This situation represents an average across a large retinal patch where light rays will intersect outer segments at random points along their axes. The estimated effective visibility found from Equation 2 has been plotted in Figure 5 for different outer segment dimensions. The drop in predicted visibility with increasing obliqueness at the retina is reminiscent of a Gaussian SCE function although some differences should again be expected due to the linearization of Equation 1. If the incident beam is rotated about the

entrance to the outer segments instead the distributions in Figure 5 narrow (not shown).

### Analytical integration of a Gaussian SCE function

Analytical integration of a Gaussian SCE function leads to an integrated visibility for normal viewing,  $\eta_{int}$ , expressed as the ratio of the effective pupil area  $A_{eff}$  (i.e., truncated with a Gaussian SCE function) with respect to that of the actual pupil area  $A_{pupil}$ :

$$\eta_{int} = \frac{A_{eff}}{A_{pupil}} = \frac{1 - 10^{-\frac{\rho^2 d_{pupil}^2}{4}}}{\frac{\rho^2 d_{pupil}^2}{4} \ln(10)} \leq 1. \quad (3)$$

This result suggests an effective limit of the pupil

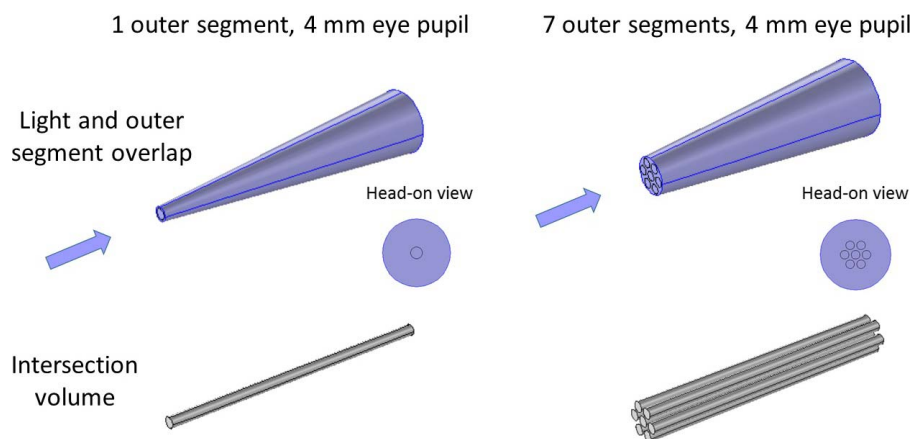


Figure 2. Volumetric overlap model simulated in COMSOL™ with one and seven hexagonally packed outer segments with light rays being incident from a 4 mm pupil onto one (left) and seven (right) adjacent identical outer segments with 50  $\mu\text{m}$  length, 2.0  $\mu\text{m}$  diameter, and 2.6  $\mu\text{m}$  spacing.

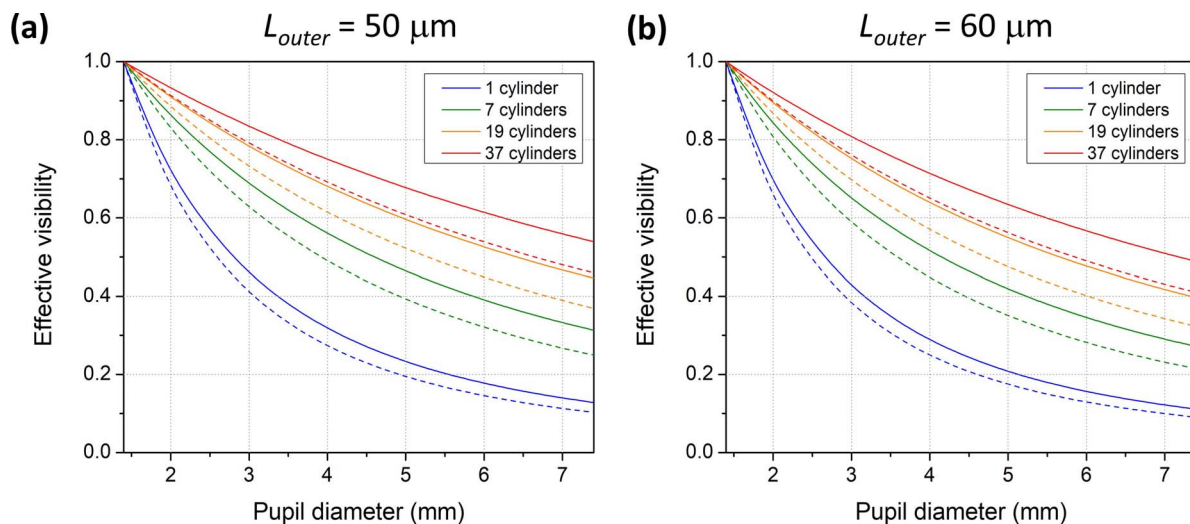


Figure 3. Effective visibility determined as intersection volume between a cone of light and cylindrical outer segments spaced by  $d_{spacing} = 1.3d_{outer}$ . The outer segment lengths are (a)  $50 \mu m$  and (b)  $60 \mu m$ , and the outer segment diameters are  $2.0 \mu m$  (solid line) and  $1.5 \mu m$  (dashed line). All plots have been normalized at  $d_{pupil} = 1.4 mm$ .

diameter to  $1.32/\sqrt{\rho}$  for large pupils (Vohnsen, 2017) and is commonly used to explain a reduced visual impact of light entering the eye near to the pupil rim.

## Experimental determination of the integrated SCE

To determine the effective visibility with pupil integration, the system shown in Figure 6 has been developed. Subjects viewed a fixation target located at 1 m distance in front of the eye with a black E-letter (3.0 mm height) printed on paper and centered within a white circle ( $\varnothing 42 mm$ ). The circle is limited by a dual layer of dark print on paper to eliminate any spurious

transmission. The target is back-illuminated by a fiber-guided halogen lamp with 150W nominal power and a 3200K spectrum (Thorlabs<sup>TM</sup> OSL1-EC). A motorized iris diaphragm (Standa<sup>TM</sup> 8MID18-1-AR) is used to set the effective pupil size, and a liquid-crystal neutral-density filter (Meadowlark<sup>TM</sup> LVA-100- $\lambda$ ) is used to match the subjective brightness for large test pupils with respect to a 1.4 mm reference pupil. A 4f telescopic system projects the motorized iris onto the eye whereby the subject sees a luminous circle covering  $\sim 4$  visual degrees through a pupil size set by the iris. The neutral-density filter has a tunable range and can attenuate up to approximately 99.9% of the incident light (3.0 ND). The color seen by the subject is set by a tunable wavelength filter (Meadowlark<sup>TM</sup> TOF-SV) with narrow bandwidth (Lochocki, Rativa, & Vohnsen, 2011).

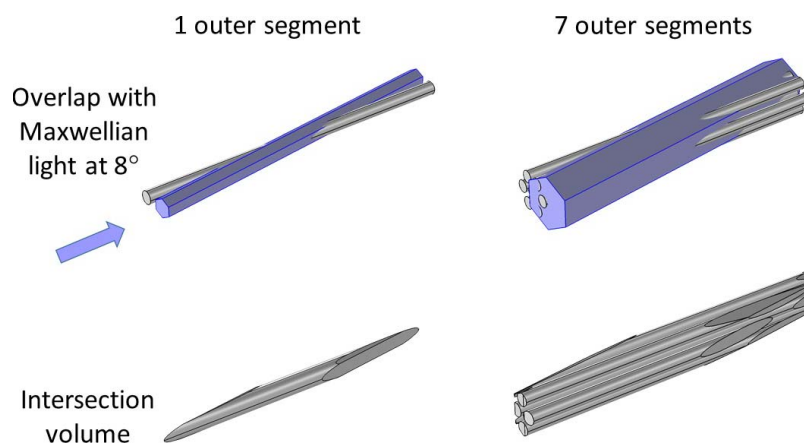


Figure 4. Volumetric overlap model simulated in COMSOL<sup>TM</sup> with a single and a group of seven adjacent outer segments with a collimated beam of light (represented by a hexagonal prism) incident at an angle of  $8^\circ$ . The shown outer segments have  $50 \mu m$  length,  $2.0 \mu m$  diameter, and  $2.6 \mu m$  spacing.

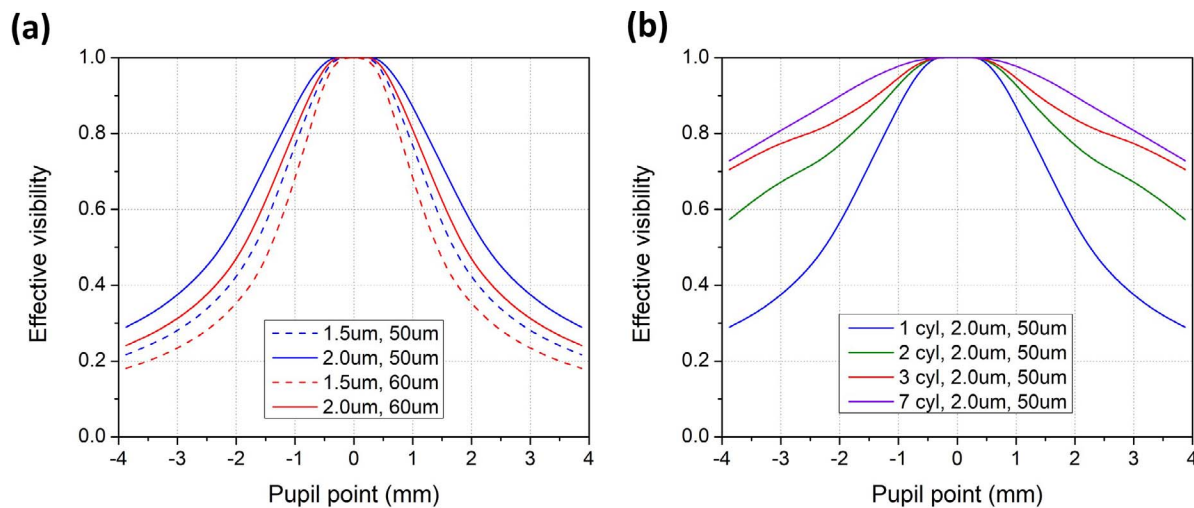


Figure 5. Effective visibility determined as intersection volume between a hexagonal prism of light representative of Maxwellian plane-wave illumination (scaled in width to match the number of outer segments) and cylindrical outer segments spaced by  $d_{\text{spacing}} = 1.3d_{\text{outer}}$ . In (a) the intersection volume with a single outer segment of length 50 μm (blue) or 60 μm (red) whereas in (b) with one (blue), two (green), three (red) and seven (purple) adjacent outer segments with 50 μm length. The diameter of each outer segment is 2.0 μm (solid line) and 1.5 μm (dashed line).

A current-driven tunable lens (Optotune™ EL-10-30-C-VIS-LD-MV) is used for subjective defocus correction at each wavelength. Prior to the psychophysical measurements, the light power reaching the eye has been calibrated using a power meter (Thorlabs™ PM100D-S120C) for different settings of the

neutral-density filter using the same configuration as in the experiments. All wavelength settings were visually inspected and spectrally characterized, and the total power transmitted by different iris-diaphragm settings was found to scale linearly with the pupil area as expected.

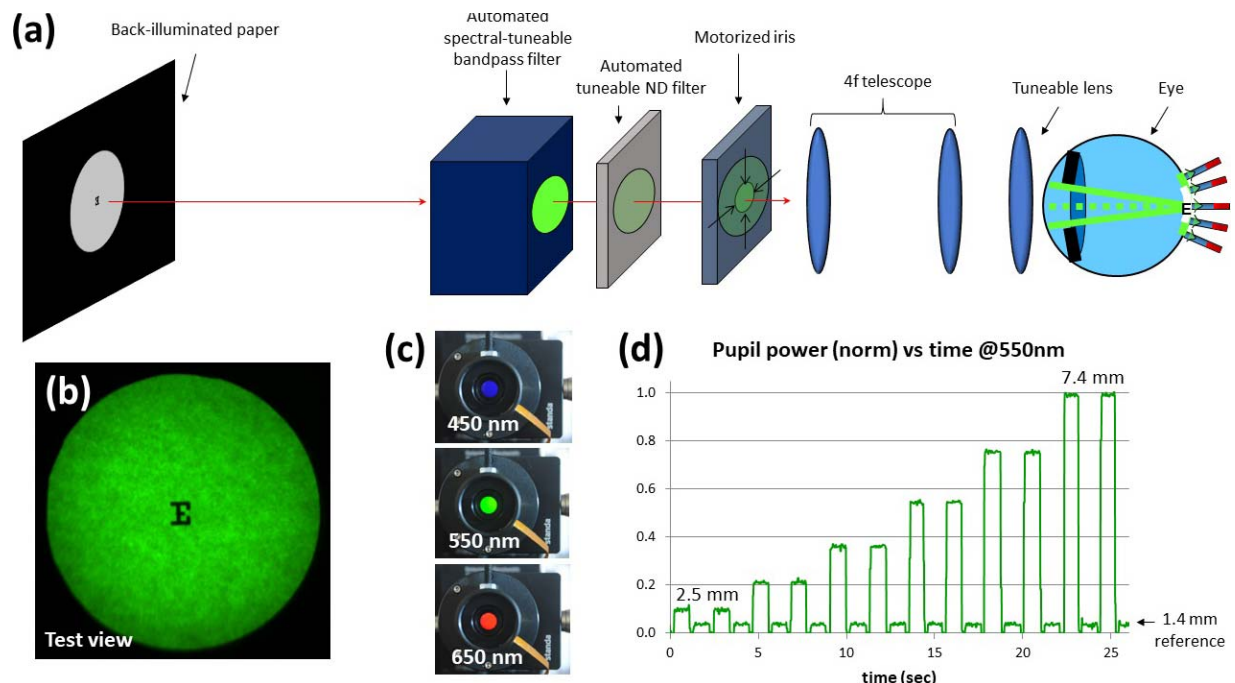


Figure 6. Experimental setup for pupil-flicker analysis of the integrated SCE including (a) schematic of the system with the E letter used for fixation, (b) view through the system of the fixation target, (c) different settings of the color bandpass filter, and (d) total power reaching the eye for increasing pupil diameters from 2.5 to 7.4 mm. A 1.4-mm iris is used as a reference pupil in the psychophysical measurements.

During the psychophysical measurements the motorized iris alternates between the reference pupil (1.4 mm) and the test pupil (from 2.5 to 7.4 mm in  $\sim 1$  mm increments) corresponding to a luminous range of up to 1.5 log units. The effective visibility is determined by the ratio

$$\eta_{\text{eff}} = A_{\text{ref}} T_{\text{ref}} / A_{\text{pupil}} T_{\text{ND}} \quad (4)$$

where  $A_{\text{ref}}$  is the area of the reference pupil (here a circle with 1.4 mm diameter),  $A_{\text{pupil}}$  is the pupil area being tested ( $\geq A_{\text{ref}}$ ),  $T_{\text{ref}}$  is the transmission of the neutral-density filter for the reference pupil, and  $T_{\text{ND}}$  is the transmission of the neutral-density filter as chosen by the subject once vision for the test and reference lights appear as equally bright.

Figure 6d shows measurements of total power transmission in the pupil plane while gradually increasing the iris size. Each chosen iris diameter is held constant for 1.0 s. To avoid sudden brightness changes, the neutral-density filter has been programmed to reduce the transmission (dark state) momentarily during the switching time of the iris which ranges from 0.1 s for small pupils to 0.3 s for large pupils; this is similar in duration to the natural eye blink. In the figure each pupil size is repeated twice, but in the psychophysical experiments each pupil-size flicker repeats continuously until a reading has been taken by the subject, which triggers the progression of the measurement series and system settings to the next test pupil size. The system is computer controlled using Labview<sup>TM</sup>, and the subject performs measurements using a numerical keypad extension while looking through the system at the fixation target.

The right eye for each author, all with normal vision, has been analyzed with the system: BV (48 years), SQ (33 years), DV (31 years), NS (26 years), and AC (26 years). A bite bar was used to minimize unwanted head motion during data collection, and subjects centered their eye for sharpest vision of the E chart after which the pupil was dilated using 1% Tropicamide. A dark patch was used to cover the left eye. Procedures are in accordance with the Declaration of Helsinki for experiments involving human subjects. The measurements were realized in two steps. First, subjects would see the fixation target through a static 4.5-mm pupil to adjust the tunable focus lens for best focus at each wavelength while fixating at the E-letter. Afterwards, the system initiated the psychophysical measurements by alternating between a 1.4-mm (reference) and 2.5-mm (test) iris in a continuous loop while allowing the subject to adjust the neutral-density filter for the test pupil until the brightness of the test and reference fields appeared as well matched. The iris would then advance to a 3.5-mm (test) and the same 1.4-mm (reference) pupil in a loop until a satisfactory brightness match was obtained, and so forth up to a 7.4-mm (test) pupil.

Once completed, the pupil-size sequence would repeat for a total of four measurement series allowing calculation of averages and deviations. A total of five wavelength settings were analyzed from 450 to 650 nm in steps of 50 nm. The entire measurement process lasted approximately 2 hr/subject including a short rest when changing wavelength to avoid fatigue.

Similar measurement series were subsequently repeated by the most experienced subject (BV) using different pupil flicker frequencies to verify that the observations were not significantly altered by temporal effects.

## Experimental results and discussion

The experimental results for the five subjects are shown in Figure 7. As can be seen, the effective visibility drops rapidly with increasing pupil size. Variations between sets of measurements are very small, with the exception of subject DV, and subject SQ who found the blue light difficult to see. With regard to the wavelength dependence, some variations can be seen, but on average the decay with pupil size is most pronounced at short wavelengths and less steep at long wavelengths. The number of S cones in the fovea are few and thus with blue light the dependence comes closest to that of the single cylindrical outer segments. In the model, this is the case of the steepest curves in Figure 3. The M and L cones are surrounded by cones of the same type or different types and are often grouped (Hofer, Singer, & Williams, 2005; Roorda & Williams, 1999) with local densities being different for each individual but typically with more L than M cones. On average, it is more likely that an L cone has another L cone as nearest neighbor than an M cone has another M cone as nearest neighbor. With more adjacent cones of the same type, the effective visibility decreases less due to the larger volume of identical visual pigments, a condition which is in qualitative agreement with the model predictions in Figure 3. The fact that the volumetric intersection model is only strictly valid for weak absorption makes the data decay slightly faster than the experimental results. A visual pigment density of 0.1 corresponds to 21% absorption whereby linearization of Equation 1 overestimates the absorption by 11%. A density of 0.3 corresponds to 50% absorption leading to a more severe overestimation by 39%. The error from linearization increases also slightly (less than 2%) with angle of incidence up to  $10^\circ$  as the propagation distance becomes larger.

Results using different pupil-size flicker frequencies for subject BV are shown in Figure 8 and confirm that the chosen frequency has little impact on the results.



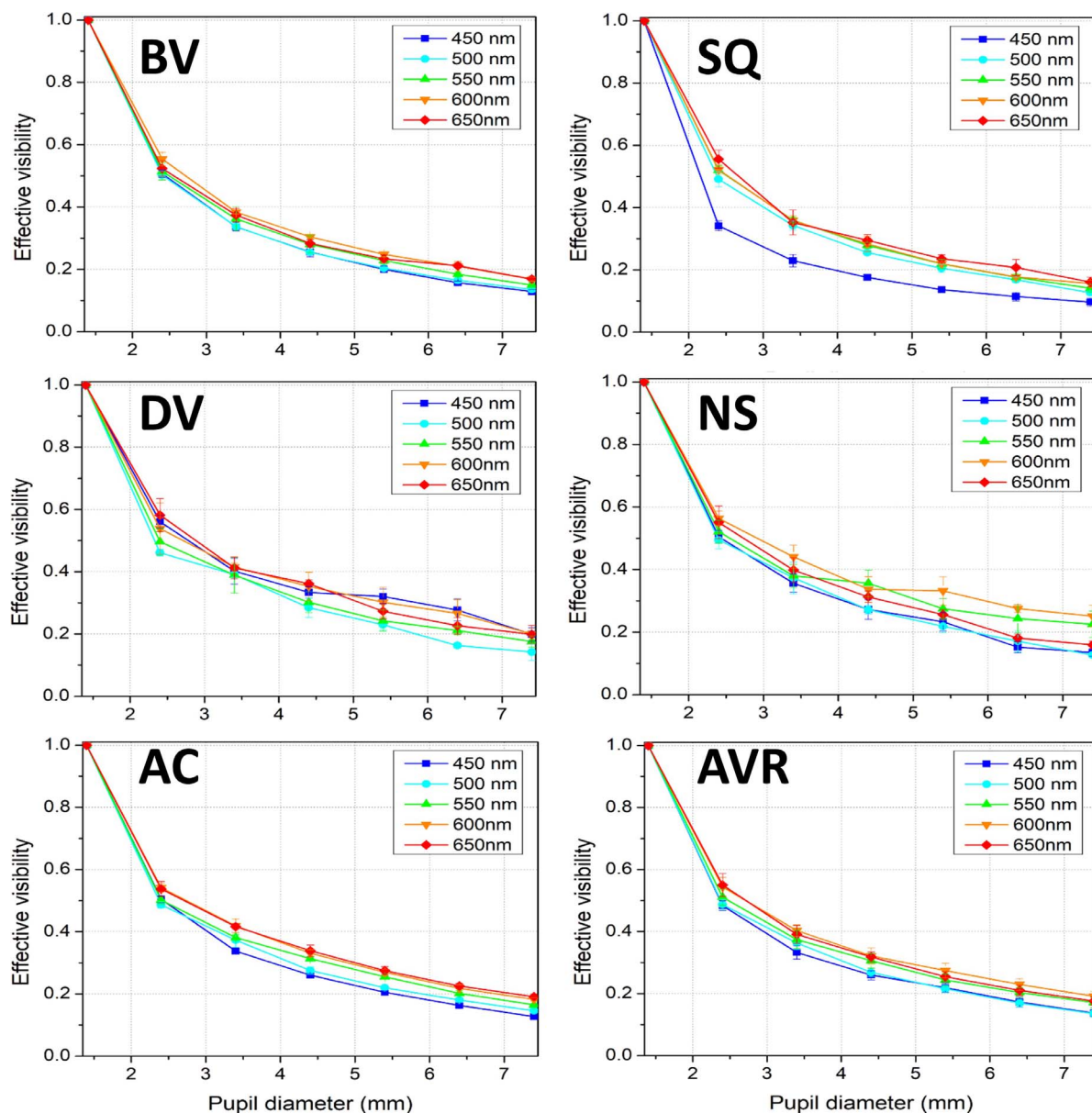


Figure 7. Experimental results obtained for the integrated visibility as a function of pupil diameter at five different wavelengths for the five subjects. Error bars indicate  $\pm 1$  SD. The average (AVR) for all subjects is also shown. All plots have been normalized at  $d_{pupil} = 1.4$  mm.

The integrated visibility data makes a significantly better fit to the volumetric intersection model presented here than direct integration of a Gaussian SCE function. This function has been included in Figure 8 for comparison. It suggests a much slower reduction in effective visibility with increasing pupil size than observed experimentally. In turn, the predictions of the volumetric intersection model make a satisfactory fit to the experimental data.

The model results for standard Maxwellian illumination SCE shown in Figure 5 suggest a fair agreement with the Gaussian SCE function. Typically a large (1–2 visual degrees) area of the fovea is illuminated for SCE characterization. This will contain individual S cones

(with the exception of the central fovea) and adjacent M and L cones with most of the latter. The effective visibility when more cones contribute will be a weighted contribution between single and multiple outer segments. The model suggests the highest directionality in the blue spectral range as S cones are not densely packed and reduced directionality at long wavelengths where the weighted average of neighboring cones flattens the predicted effective visibility. This spectral tendency of the SCE directionality was also observed in Stiles' data (1937). The results for a single cone shown in Figure 5a fit a Gaussian directionality with  $\rho$  in the range of  $0.049/\text{mm}^2$  (for  $50\ \mu\text{m}$  length and  $2.0\ \mu\text{m}$  diameter) to  $0.100/\text{mm}^2$  (for  $60\ \mu\text{m}$  length and  $1.5\ \mu\text{m}$



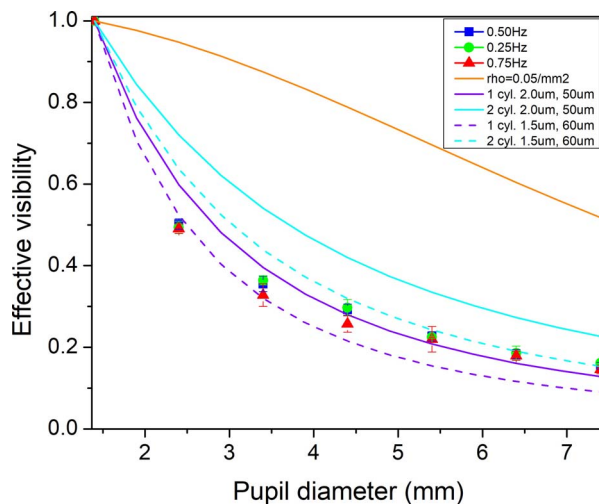


Figure 8. Experimental results obtained for the integrated visibility as a function of pupil diameter using the right eye for subject BV at three different flicker frequencies equal to, slower, and faster than the measurements in Figure 7: 0.50 Hz (blue squares), 0.25 Hz (green circles), and 0.75 Hz (red triangles). The error bars indicate  $\pm 1$  SD for a total of four measurement series at 550 nm wavelength. The data fit closely to the volumetric intersection volume between one (violet solid and dashed line) and two (cyan solid and dashed line) adjacent outer segments with length between 50  $\mu\text{m}$  and 60  $\mu\text{m}$  and diameter between 1.5  $\mu\text{m}$  and 2.0  $\mu\text{m}$ . For comparison, an integrated Gaussian SCE function with directionality  $\rho = 0.05/\text{mm}^2$  is shown (orange line). All plots have been normalized at  $d_{\text{pupil}} = 1.4$  mm.

diameter). These values are in good agreement with expectations from the literature (Applegate & Lakshminarayanan, 1993; Lochocki & Vohnsen, 2013; Stiles & Crawford, 1933). When groups of adjacent cones contribute the estimated directionality from Figure 5b is 0.049/ $\text{mm}^2$  (one cone), 0.019/ $\text{mm}^2$  (two cones), 0.012/ $\text{mm}^2$  (three cones), and 0.010/ $\text{mm}^2$  (seven cones), but the actual foveal cone distribution will result in a weighted average of these values. In consequence, the volumetric intersection model also suggests a plausible explanation for the much diminished parafoveal rod directionality since these cells are surrounded by the same cell type. Leakage between rods will flatten the effective visibility versus angle of incidence, causing a lack of directionality for scotopic vision.

## Conclusions

A volumetric intersection model has been introduced that to a first approximation excludes waveguiding and gives support to a geometrical optics interpretation of vision in terms of the fraction of absorbed light. The analysis has been used to elucidate how efficiently light

stimulates a visual sensation. Direct determination of the integrated SCE in normal viewing situations has been realized using pupil-size flickering for five subjects. We have found good correspondence between the volumetric intersection model and the experimental results of pupil integration whereas integration of a standard SCE function is in disagreement with the experimental observations for nonMaxwellian illumination. The results emphasize the need to incorporate the SCE in accurate eye modeling such as in the design of intraocular lenses (Norrby, Piers, Campbell, & van der Mooren, 2007). The rapid reduction of integrated visibility for small pupils may also be relevant for aperture inlays used in the treatment of presbyopia (Tabernero & Artal, 2012). It is important for the development of improved retinal models that better relate calculated retinal images to vision by taking the detailed photonic structure of the retina and pigments into account (Vohnsen, 2014) and where the geometrical optics absorption model in combination with wave models including both guided and nonguided components should ultimately provide a more accurate description. We are conducting further research in this area to bridge the geometrical approach presented here with more detailed electromagnetic light propagation analysis.

**Keywords:** Stiles-Crawford effect of the first kind, cone photoreceptors, visibility, integrated Stiles-Crawford effect, absorption, geometrical optics

## Acknowledgments

This research has been realized with financial support by the H2020 ITN MyFUN grant agreement no. 675137, Capes Foundation Science without Borders, and the King Abdullah scholarship program. The authors are grateful to Benjamin Lochocki for help at the early stages of the experimental realization.

Commercial relationships: none.

Corresponding author: Brian Vohnsen.

Email: brian.vohnsen@ucd.ie.

Address: Advanced Optical Imaging Group, School of Physics, University College Dublin, Dublin, Ireland.

## References

- Applegate, R. A., & Lakshminarayanan, V. (1993). Parametric representation of Stiles-Crawford functions: Normal variation of peak location and directionality. *Journal of the Optical Society of America A*, 10, 1611–1623.

- Bowmaker, J. K., & Dartnall, H. J. A. (1980). Visual pigments of rods and cones in a human retina. *Journal of Physiology*, 298, 501–511.
- Burns, S. A., Wu, S., Delori, F., & Elsner, A. E. (1995). Direct measurement of human-cone-photoreceptor alignment. *Journal of the Optical Society of America A*, 12, 2329–2338.
- Castillo, S., & Vohnsen, B. (2013). Exploring the Stiles-Crawford effect of the first kind with coherent light and dual Maxwellian sources. *Applied Optics*, 52, A1–A8.
- Chen, B., & Makous, W. (1989). Light capture by human cones. *Journal of Physiology*, 414, 89–109.
- Curcio, C. A., Sloan, K. R., Kalina, R. E., & Hendrickson, A. E. (1990). Human photoreceptor topography. *Journal of Comparative Neurology*, 292, 497–523.
- Delint, P. J., Berendschot, T. T. J. M., & van Norren, D. (1997). Local photoreceptor alignment measured with a scanning laser ophthalmoscope. *Vision Research*, 37, 243–248.
- dos Santos, D. V., & Vohnsen, B. (in press). Retina-simulating phantom produced by chemically amplified photolithography. *Optics Letters*, in press.
- Drum, B. (1975). Additivity of the Stiles-Crawford effect for a Fraunhofer image. *Vision Research*, 15, 291–298.
- Elsner, A. E., Berk, L., Burns, S. A., & Rosenberg, P. R. (1988). Aging and human cone photopigments. *Journal of the Optical Society of America A*, 5, 2106–2112.
- Elsner, A. E., Burns, S. A., & Webb, R. H. (1993). Mapping cone photopigment optical density. *Journal of the Optical Society of America A*, 10, 52–58.
- Enoch, J. M. (1958). Summated response of the retina to light entering different parts of the pupil. *Journal of the Optical Society of America A*, 48, 392–405.
- Enoch, J. M. (1963). Optical properties of the retinal receptors. *Journal of the Optical Society of America*, 53, 71–85.
- Enoch, J. M., & Lakshminarayanan, V. (2009). Integration of the Stiles-Crawford effect of the first kind. *Journal of Modern Optics*, 20, 2240–2250.
- Ercoles, A. M., Ronchi L., & Toraldo di Francia, G. (1956). The relation between pupil efficiencies for small and extended pupils of entry. *Optica Acta*, 3, 84–89.
- Gao, W., Cense, B., Zhang, Y., Jonnal, R. S., & Miller, D. T. (2008). Measuring retinal contributions to the optical Stiles-Crawford effect with optical coherence tomography. *Optics Express*, 16, 6486–6501.
- Gorrand, J.-M., & Delori, F. (1995). A reflectometric technique for assessing photoreceptor alignment. *Vision Research*, 35, 999–1010.
- Hofer, H., Singer, B., & Williams, D. R. (2005). Different sensations from cones with the same photopigment. *Journal of Vision*, 5(5):5, 444–454, doi:10.1167/5.5.5. [PubMed] [Article]
- Kilbride, P. E., Read, J. S., Fishman, G. A., & Fishman, M. (1983). Determination of human cone pigment density difference spectra in spatially resolved regions of the fovea. *Vision Research*, 23, 1341–1350.
- Lochocki, B., Rativa, D., & Vohnsen, B. (2011). Spatial and spectral characterization of the first and second Stiles-Crawford effects using tuneable liquid-crystal filters. *Journal of Modern Optics*, 58, 1817–1825.
- Lochocki, B., & Vohnsen, B. (2013). Defocus-corrected analysis of the foveal Stiles-Crawford effect of the first kind across the visible spectrum. *Journal of Optics*, 15, 125301.
- Lochocki, B., & Vohnsen, B. (2017). Uniaxial flicker analysis of the psychophysical Stiles-Crawford effects. *Journal of Modern Optics*, 64, 347–356.
- Marcos, S., & Burns, S. A. (1999). Cone spacing and waveguide properties from cone directionality measurements. *Journal of the Optical Society of America A*, 16, 995–1004.
- Marcos, S., Burns, S. A., & He, J. C. (1998). Model for cone directionality reflectometric measurements based on scattering. *Journal of the Optical Society of America A*, 15, 2012–2022.
- Morris, H. J., Blanco, L., Codona, J. L., Li, S., Choi, S. S., & Doble, N. (2015). Directionality of individual cone photoreceptors in the parafoveal region. *Vision Research*, 117, 67–80.
- Norrby, S., Piers, P., Campbell, C., & van der Mooren, M. (2007). Model eyes for evaluation of intraocular lenses. *Applied Optics*, 46, 6595–6605.
- Packer, O. S., Williams, D. R., & Bensinger, D. G. (1996). Photopigment transmittance imaging of the primate photoreceptor mosaic. *Journal of Neuroscience*, 16, 2251–2260.
- Pircher, M., Göttinger, E., Sattmann, H., Leitgeb, R. A., & Hitzenberger, C. K. (2010). In vivo investigation of human cone photoreceptors with SLO/OCT in combination with 3D motion correction on a cellular level. *Biomedical Optics Express*, 18, 13935–13944.
- Rativa, D., & Vohnsen, B. (2011). Analysis of individual cone-photoreceptor directionality using scanning laser ophthalmoscopy. *Biomedical Optics Express*, 2, 1423–1431.

- Roorda, A., & Williams, D. R. (1999). The arrangement of the three cone classes in the living human eye. *Nature*, 397, 520–522.
- Roorda, A., & Williams, D. R. (2002). Optical fiber properties of individual human cones. *Journal of Vision*, 2(5):4, 404–412, doi:10.1167/2.5.4. [PubMed] [Article]
- Sidman, R. L. (1957). The structure and concentration of solids in photoreceptor cells studied by refractometry and interference microscopy. *Journal of Biophysical and Biochemical Cytology*, 3, 15–30.
- Snyder A. W., & Pask, C. (1973). The Stiles-Crawford effect-explanation and consequences. *Vision Research*, 13, 1115–1137.
- Stiles, W. S. (1937). The luminous efficiency of monochromatic rays entering the eye pupil at different points and a new colour effect. *Proceedings of the Royal Society B*, 123, 90–118.
- Stiles, W. S., & Crawford, B. H. (1933). The luminous efficiency of rays entering the eye pupil at different points. *Proceedings of the Royal Society B*, 112, 428–450.
- Tabernero, J., & Artal, P. (2012). Optical modeling of a corneal inlay in real eyes to increase depth of focus: Optimum centration and residual defocus. *Journal of Cataract and Refractive Surgery*, 38, 270–277.
- Torraldo di Francia, G. (1948). Per una teoria dell'effetto Stiles-Crawford [Translation: For a theory of the Stiles-Crawford effect]. *Nuovo Cimento*, 5, 589–590.
- van Blokkland, G. J. (1986). Directionality and alignment of the foveal receptors assessed with light scattered from the human fundus in vivo. *Vision Research*, 26, 495–500.
- Van Loo, J. A., Jr., & Enoch, J. M. (1975). The scotopic Stiles-Crawford effect, *Vision Research*, 15, 1005–1009.
- Vohnsen, B. (2007). Photoreceptor waveguides and effective retinal image quality. *Journal of the Optical Society of America A*, 24, 597–607.
- Vohnsen, B. (2014). Directional sensitivity of the retina: A layered scattering model of outer-segment photoreceptor pigments. *Biomedical Optics Express*, 5, 1569–1587.
- Vohnsen, B. (2017). The retina and the Stiles-Crawford effects. In P. Artal (Ed.), *Handbook of visual optics* (Vol. 1, pp. 257–276). Boca Raton, FL: Taylor & Francis.
- Vohnsen, B., Iglesias, I., & Artal, P. (2005). Photoreceptor waveguides and effective retinal image quality. *Journal of the Optical Society of America A*, 22, 2318–2328.
- Vohnsen, B., & Rativa, D. (2011). Absence of an integrated Stiles-Crawford function for coherent light. *Journal of Vision*, 11(1):19, 1–10, doi:10.1167/11.1.19. [PubMed] [Article]
- Walraven, P. L., & Bouman, M. A. (1960). Relation between directional sensitivity and spectral response curves in human cone vision. *Journal of the Optical Society of America*, 50, 780–784.
- Westheimer, G. (2013). Retinal light distributions, the Stiles-Crawford effect and apodization. *Journal of the Optical Society of America A*, 30, 1417–1421.
- Williams, D. R., MacLeod, D. I. A., & Hayhoe, M. M. (1981). Foveal tritanopia. *Vision Research*, 21, 1341–1356.
- Wyszecki, G., & Stiles, W. S. (1980). High-level trichromatic color matching and the pigment-bleaching hypothesis. *Vision Research*, 20, 23–37.